

COMSOL Multiphysics¹ Simulation of 3D Single-Phase Transport in a Random Packed Bed of Spheres

A0G. Dixon^{*1}

¹Department of Chemical Engineering, Worcester Polytechnic Institute, Worcester, MA, USA

*Corresponding author: agdixon@wpi.edu

Abstract: COMSOL Multiphysics was used for detailed simulations of flow, heat transfer and dispersion in a 400-sphere random fixed bed of tube-to-particle diameter ratio $N = 5.96$. Simulations were carried out in both laminar ($50 \leq Re \leq 400$) and turbulent ($400 \leq Re \leq 5000$) flow regimes. Details of flow in the packing such as regions of fast flow and back flow are presented, as well as comparisons of pressure drop to well-established correlations. Simulations were extended to include conjugate heat transfer where the tube was heated from the wall and show the developing temperature profile within the gas phase and the alumina particles, due to conduction and convection. Finally, isothermal simulations were run of a tracer source at the tube inlet to show the radial dispersion of mass caused by lateral displacement of flow around the packing.

Keywords: Computational fluid dynamics, packed bed, heat transfer, dispersion, sphere pack.

1. Introduction

Packed beds are important in the chemical industries in separations and as catalytic reactors. The standard approach to modeling the complex particle/tube arrangement in a packed bed is to employ an effective medium approach with one-dimensional flow and lumped transport parameters. Simplification of the flow and estimation of the transport quantities is usually done by experiment and empiricism. Computational fluid dynamics (CFD) can be used to simulate the detailed flow and scalar transport in packed beds to provide improved understanding and quantitative information, for use in developing the effective medium models that are the basis for chemical reactor analysis.

The aim of the present work is to use COMSOL Multiphysics to perform detailed simulations of flow, heat transfer and dispersion in fixed beds of spheres of tube-to-particle diameter ratio (N) in the range 3 – 10 which is

commonly used for reactions such as steam reforming where strong heat effects and the corresponding cooling requirements and the need to reduce pressure drop lead to the use of large particles in thin tubes. Specialized finite volume CFD tools have been used previously for 3D simulations [1 – 5], mainly for flow and heat transfer only, while studies using finite element methods such as COMSOL Multiphysics have so far been restricted to 2D simulations [6, 7] or small structured clusters of spheres [8]. Here we present simulations of single-phase gas flow, conjugate heat transfer and isothermal dispersion of mass in a 3D model of a randomly-packed bed ($N = 5.96$) of 400 spheres.

2. Model Equations

Due to the complex nature of the fluid region between the particles, there was no symmetry in this model and the full 3D equations had to be solved. The simulations were all run at steady-state.

2.1 Equation of Continuity

The fluid was at atmospheric pressure and so it was taken as being incompressible (constant density). The continuity equation then becomes

$$\nabla \cdot \mathbf{u} = 0 \quad (1)$$

2.2 Navier-Stokes Equations

The fluid was Newtonian (air) with constant density $\rho = 1.225 \text{ kg/m}^3$ and viscosity $\mu = 1.789 \times 10^{-5} \text{ Pa}\cdot\text{s}$ resulting in the Navier-Stokes equations (for laminar flow):

$$\rho(\mathbf{u} \cdot \nabla)\mathbf{u} = \nabla \cdot [-p\mathbf{I} + \mu(\nabla\mathbf{u} + (\nabla\mathbf{u})^T)] + \mathbf{F} \quad (2)$$

For laminar flow the boundary conditions were zero velocity (no-slip) on all particles and the tube wall, a flat inlet velocity v_{in} at the tube entrance, and the “pressure, no viscous stress” condition at the tube exit. For turbulent flow the

usual extra terms involving turbulent viscosity and turbulent kinetic energy appear. For wall boundaries a wall function condition was applied.

2.3 Standard k - ε Turbulence Model

The transition from laminar to turbulent flow in a packed bed has been a matter of some debate. The consensus appears to be that steady laminar flow persists up to a Reynolds number ($Re = \rho d_p U / \mu$) of about 60, followed by an unstable laminar flow with unsteady wake oscillations which is succeeded as Re increases by an unsteady chaotic inertial flow that qualitatively resembles turbulent flow once $Re > 120$ -150 [9]. It is agreed that the transition to true turbulence is gradual and may not be reached until $Re > 900$ -1000 [10]. In this study, we used laminar flow until difficulty was found in converging the equations at higher Re , then we switched to the standard RANS k - ε model given by the turbulent kinetic energy equation

$$\rho(\mathbf{u} \cdot \nabla)k = \nabla \cdot \left(\left[\mu + \frac{\mu_T}{\sigma_k} \right] \nabla k \right) + P_k - \rho\varepsilon \quad (3)$$

and the dissipation rate equation

$$\rho(\mathbf{u} \cdot \nabla)\varepsilon = \nabla \cdot \left(\left[\mu + \frac{\mu_T}{\sigma_\varepsilon} \right] \nabla \varepsilon \right) + C_{e1}P_k \frac{\varepsilon}{k} - C_{e2}\rho \frac{\varepsilon}{k^2} \quad (4)$$

In these equations P_k is

$$P_k = \mu_T [\nabla \mathbf{u} : (\nabla \mathbf{u} + (\nabla \mathbf{u})^T)] \quad (5)$$

The turbulent viscosity was given by

$$\mu_T = \rho C_\mu \frac{k^2}{\varepsilon} \quad (6)$$

where C_{e1} , C_{e2} and C_μ are turbulence model constants, and σ_k and σ_ε are the turbulent Prandtl numbers for k and ε respectively.

2.4 Heat Transfer

The energy equation took the form

$$\rho C_p \mathbf{u} \cdot \nabla T = \nabla \cdot (k \nabla T) + Q \quad (7)$$

for the fluid, where k is the thermal conductivity of air (= 0.0242 W/m·K) and the source term Q

was zero. For the conjugate heat transfer in the solid particles the equation became

$$0 = \nabla \cdot (k \nabla T) + Q \quad (8)$$

In this case $k = 1.0$ W/m·K, typical for alumina, a common catalyst support material. The source term was again zero. For boundary conditions, the inlet temperature was set to 293.15 K, the tube wall was held at 373.15 K and the tube outlet was zero conductive flux.

2.5 Species Transport

For the mass transfer simulations a single generic species was used, resulting in the species balance equation

$$\nabla \cdot (-D_i \nabla c_i) + \mathbf{u} \cdot \nabla c_i = R_i \quad (9)$$

The species diffusivity was taken as $D_i = 1 \times 10^{-5}$ m²/s and the reaction rate term R_i was zero. For boundary conditions zero species flux was set on all walls, and the tube outlet was zero diffusive flux. At the inlet a finite-area source was used as described in the following section.

3. Use of COMSOL Multiphysics

A random pack of spheres was generated by a Monte Carlo collective re-arrangement algorithm and validated [1], and the geometry was imported into COMSOL Multiphysics 4.3b using the CAD Import Module (see Figure 1).



Figure 1. 400-sphere packed bed with $N = 5.96$.

The tube was 0.07569 m in diameter and packed length was 0.3467 m, with 0.0254 m of empty tube between the inlet and the bed and 0.0508 m between the bed and the outlet.

The spheres were nominally 0.0254 m in diameter, leading to a nominal void fraction of 0.4501. Contact points between the spheres were avoided by shrinking the particles by 1% of their diameters. The actual void fraction was then 0.4682, an error of 4%. From past experience, this would be expected to result in pressure drops low by 10-12%. The size of the model forced the use of coarse (411,000 elements - laminar) and extra coarse (352,000 elements - turbulent) meshes (Figure 2).



Figure 2. Coarse (left) and Extra coarse (right) meshes.

The flow simulations used Laminar and Turbulent flow ($k-\epsilon$ with wall functions) physics. The conjugate heat transfer problem used the Heat Transfer Module where the Heat Transfer in Fluids model was first set up then the Heat Transfer in Solids model was added to it, which ensured that the two models coupled temperature and flux correctly across the fluid-solid interface. Dispersion of mass was handled in the Transport of Dilute species model. The inlet source was implemented by defining two rectangular functions, one in x and one in y where the rectangle width was 0.006 m for laminar flows but the coarser mesh in turbulent flows required the width to be increased to 0.012m. The simulations were converged by using the segregated solution algorithm, first running a study for flow alone and using the results to set initial values for flow in the subsequent study of simultaneous flow and heat or mass transfer.

4. Results and Discussion

For each of the three cases reported here a total of nine values of Re were run, four under laminar flow and five under turbulent flow. The values are given in Table 1 along with the corresponding pressure drops, in the Appendix.

4.1 Fluid Flow

The flow distributions inside the bed of particles were similar for all flow rates, with only the magnitudes changing. A sample set of contours of axial velocity for laminar flow are shown in Figure 3, where the set of slices through the bed give an impression of the distribution of velocities in 3D, while the 2D contours on the mid-tube plane ($x = 0$) show details of the flow more clearly.

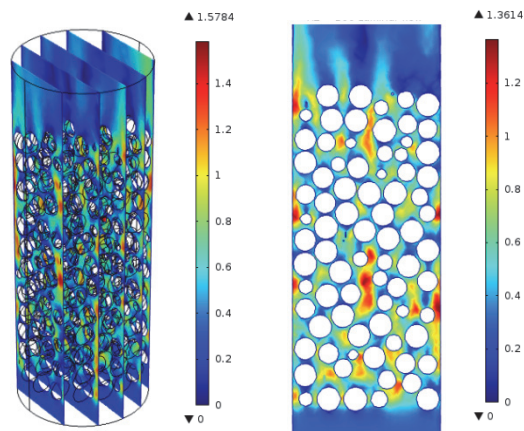


Figure 3. Axial velocity w : 3D view on slices (left) and 2D contour plot (right) through mid-tube. $Re = 100$ (laminar)

It is clear to see that there are regions of accelerated flow between the particles, some at the center of the tube and some at the tube wall, where the higher void fraction is expected to result in flow by-passing. Regions of low and negative flow are also seen, usually in the wake of the spheres. It is notable that the flow at the exit of the bed is completely different from that inside the bed, suggesting that experimental measurements of velocity made downstream of the bed exit could be in substantial error. This observation would reinforce the argument that non-invasive measurements inside the packing, for example by MRI, are necessary.

An example of turbulent flow is presented in Figure 4, where the 2D contour shows the overall similarities to the laminar case. A 3D map of pressure is also given, showing the decrease in the axial direction while the pressure is fairly constant over the cross-section perpendicular to flow, although fluctuations at the local level can be seen.

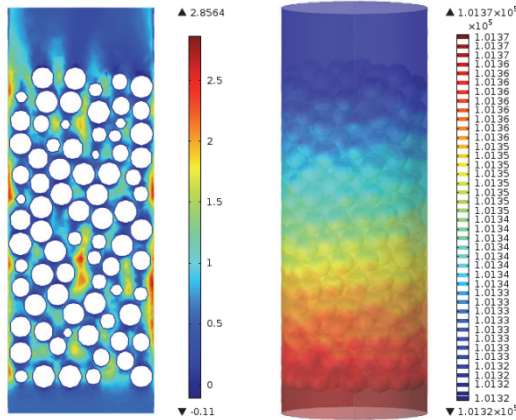


Figure 4. Axial velocity w : 2D contour plot (left) through mid-tube; and 3D plot of pressure (right). $Re = 1000$ (turbulent).

The pressure drops are given in Table 1, where they are compared to the predictions of the well-known correlation given by Eisfeld and Schnitzlein [11] which is based on the Ergun equation but contains corrections for wall effects. Overall agreement is good with errors below 5% for the laminar cases and the lower turbulent runs, but rising to as much as 25% at the higher flow rates. This is too high to be accounted for by the increased void fraction, and is most likely due to using too coarse a mesh as turbulence becomes more pronounced.

4.2 Heat Transfer

Simulations were next extended to include conjugate heat transfer where cold air flowing through the tube was heated from the constant-temperature wall. Figure 5 shows the developing temperature profile within the gas and the particles for a relatively high flow rate in the turbulent regime.

The different thermal conductivities of the particles and the fluid lead to irregular

temperature isotherms, which are also affected by the radial displacement of the fluid flow.

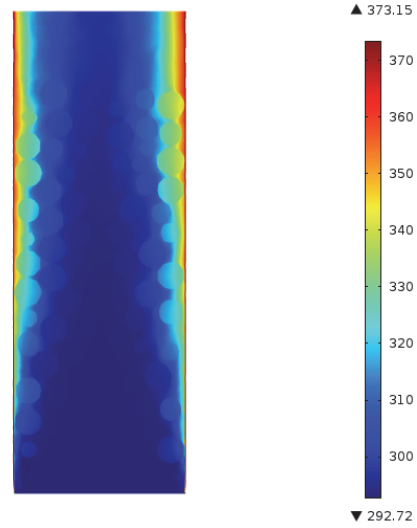


Figure 5. 2D contour plot of temperature on midplane. $Re = 1000$ (turbulent).

A second illustration of the temperature field development is provided in Figure 6, this time for laminar flow. A much greater penetration of the temperature into the bed can be seen due to the slower flow rate which allows the gas to heat to a greater extent within the limits of the bed. By defining suitable radial surfaces, these simulations could be used to provide radial temperature profiles which could yield estimates of effective heat transfer parameters.

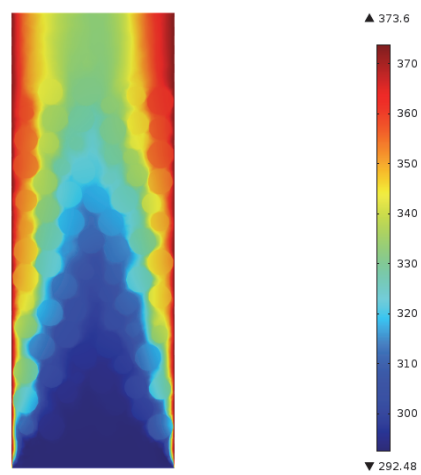


Figure 6. 2D contour plot of temperature on midplane. $Re = 100$ (laminar).

An alternative view of the temperature contours is given in Figure 7, looking down the bed in the axial direction. This view emphasizes the irregular nature of the temperature field. For example, the cold region in the center is offset from the tube axis due to the arrangement of the particles, where an axial channel funnels colder air that has not been heated as much by contact with the warmer particles.

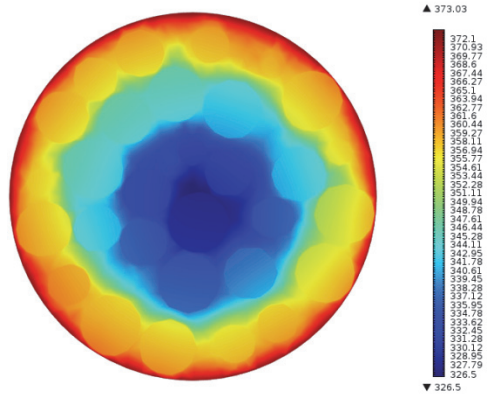


Figure 7. 2D contour plot of temperature on cross-section $z = 0.30$ m. $Re = 100$ (laminar).

4.3 Mass Transfer

Finally, isothermal simulations were run of a tracer source at the tube inlet to show the radial dispersion of mass caused by lateral displacement of flow around the packing (Figure 8). The source is not a perfect step function in 2D, but has spread a little in only a short distance.

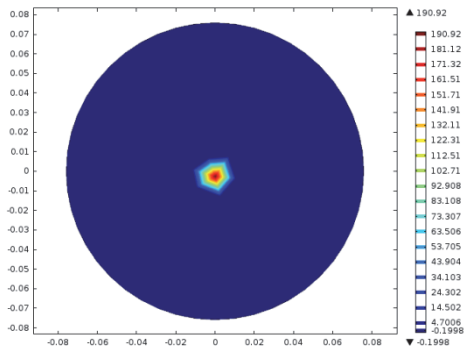


Figure 8. 2D contour plot of concentration on cross-section $z = 0.0127$ m, just above mass source at inlet. $Re = 200$ (laminar).

The dispersion of the species under laminar flow is shown in Figure 9. Note that the slower flow has allowed the concentration to be reduced quite quickly at the inlet (c_{in} is 200 mol/m³).

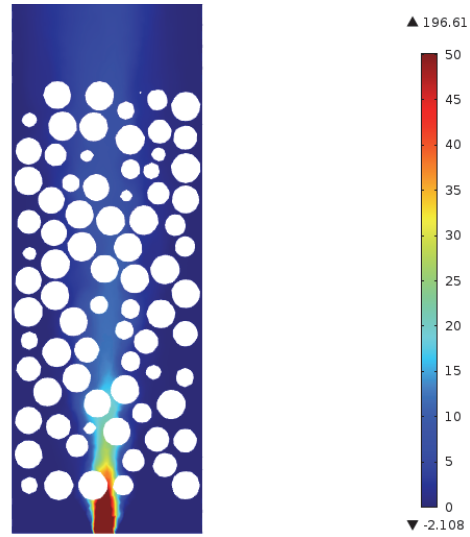


Figure 9. 2D contour plot of concentration on midplane, showing mass source at inlet and dispersion of mass in the packing. $Re = 200$ (laminar).

A similar plot is presented for turbulent flow in Figure 10; notice the difference in color scale.

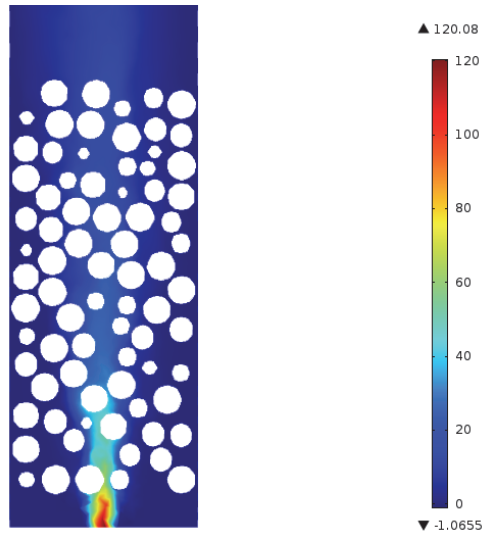


Figure 10. 2D contour plot of concentration on midplane, showing mass source at inlet and dispersion of mass in the packing. $Re = 1000$ (turbulent).

The inlet concentration is reduced to a lesser extent in the faster flow. Surface integration was performed to check on the material balance closure, which was good to 5% except for the two highest flows; again an overly coarse mesh was the most likely cause. Point evaluations showed that as flow rate increased the exit concentration at the bed axis increased while that at the tube wall decreased. Again, radial concentration profiles could be obtained to estimate radial dispersion coefficients.

5. Conclusions

COMSOL Multiphysics 4.3b was used successfully to simulate flow and transport over a wide range of flow rates in a realistic 3D packed bed of spheres. Future research will look at the inclusion of simultaneous heat and mass transfer and chemical reactions.

6. References

1. Behnam, M.; Dixon, A. G.; Nijemeisland, M.; Stitt, E. H., A new approach to fixed bed radial heat transfer modeling using velocity fields from computational fluid dynamics simulations, *Ind. Eng. Chem. Res.*, **52**, 15244-15261 (2013)
2. Augier, F.; Idoux, F.; Delenne, J. Y., Numerical simulations of transfer and transport properties inside packed beds of spherical particles, *Chem. Eng. Sci.*, **65**, 1055-1064 (2010)
3. Baker, M. J.; Tabor, G. R., Computational analysis of transitional air flow through packed columns of spheres using the finite volume technique, *Comput. Chem. Eng.*, **34**, 878-885 (2010)
4. Eppinger, T.; Seidler, K.; Kraume, M., DEM-CFD simulations of fixed bed reactors with small tube to particle diameter ratios, *Chem. Eng. J.*, **166**, 324-331 (2011).
5. Atmakidis, T.; Kenig, E. Y., Numerical analysis of mass transfer in packed-bed reactors with irregular particle arrangements, *Chem. Eng. Sci.*, **81**, 77-83 (2012).
6. Varela, A. E.; Garcia, J. C., Multiphysics simulation of a packed bed reactor, Proceedings of the COMSOL Conference, Boston (2009)
7. Rádi, Gy.; Varga, T.; Chován, T., Catalytic pellet based heterocatalytic reactor bed models development, Proceedings of the COMSOL Conference, Paris (2010)
8. Sachdev, S.; Pareek, S.; Mahadevan, B.; Deshpande, A., Modeling and simulation of single phase flow and heat transfer in packed beds, Proceedings of the COMSOL Conference, Bangalore (2012)
9. Dybbs, A.; Edwards, R. V., A new look at porous media fluid mechanics - Darcy to turbulent. In J. Bear M. Corapcioglu, *Fundamentals of transport phenomena in porous media* (p. 201), Martinus Nijhoff (1984)
10. Seguin, D.; Montillet, A.; Comiti, J.; Huet, F., Experimental characterization of flow regimes in various porous media - II: Transition to turbulent regime, *Chem. Eng. Sci.*, **53**, 3897-3909 (1998)
11. Eisfeld, B.; Schnitzlein, K., The influence of containing walls on the pressure drop in packed beds, *Chem. Eng. Sci.*, **56**, 4321-4329 (2001)

7. Acknowledgements

Two WPI undergraduates contributed to the developments reported in this paper. Brandon C. Bukowski modeled fluid flow, heat and mass transfer for a single sphere in a tube. Michael Chase imported models for $N = 3$ and $N = 5.96$ into COMSOL and carried out preliminary simulations of flow and heat transfer.

8. Appendix

Table 1: Pressure drop comparison to literature

Re	$-\frac{\Delta P}{L}$ (Pa/m) calculated	$-\frac{\Delta P}{L}$ (Pa/m) Reference [11]
50	0.811	0.8025
100	2.305	2.219
200	7.009	6.894
400 (lam.)	22.476	23.611
400 (turb.)	27.037	23.611
600	52.179	50.152
800	84.636	86.516
1000	124.27	132.703
2000	427.34	510.99
5000	2340.2	3119.35